Photocatalysis

CuCo$_2$S$_4$ Deposited on TiO$_2$: Controlling the pH Value Boosts Photocatalytic Hydrogen Evolution

Michael Poschmann,[a] Hendrik Groß,[b] Reza Amin,[c] Charlotte Fritsch,[d] Torben Dankwort,[b] Hannes Radinger,[d] Sylvio Indris,[d] Lorenz Kienle,[b] and Wolfgang Bensch*[a]

Abstract: Metallic spinel-type CuCo$_2$S$_4$ nanoparticles were deposited on nanocrystalline TiO$_2$ (P25®), forming heterostructure nanocomposites. The nanocomposites were characterized in detail by X-ray powder diffraction (XRD), high-resolution transmission electron microscopy (HRTEM), nitrogen sorption (BET) and UV/Vis spectroscopy. Variation of the CuCo$_2$S$_4$:TiO$_2$ ratio to an optimum value generated a catalyst which shows a very high photocatalytic H$_2$ production rate at neutral pH of 32.3 μmol/h (0.72 mL h^{-1}), which is much larger than for pure TiO$_2$ (traces of H$_2$). The catalyst exhibits an extraordinary long-term stability and after 70 h irradiation time about 2 mmol H$_2$ were generated. An increased light absorption and an efficient charge separation for the sample with the optimal CuCo$_2$S$_4$:TiO$_2$ ratio is most probably responsible for the high catalytic activity.

Introduction

The necessity to reduce or even avoid greenhouse gas emissions encourages intense efforts for the development of alternative, eco-friendly and renewable fuels. Widely discussed processes are the catalytic hydrogen evolution by either water splitting or using sacrificial agents,[1–9] biorefinery,[10,11] CO$_2$ fixation[12,13] or CO$_2$ conversion into value added chemicals or fuels.[14,15] Nowadays, hydrogen gas is produced mainly by steam reforming/water-gas shift reaction using natural gas, which is neither renewable nor eco-friendly. Eco-friendly catalytic hydrogen evolution can be achieved by electrocatalysis, photocatalysis or the combined photo-electro-catalysis.[1] A promising reaction is the photocatalytic water splitting [Equation (1) and Figure 1) applying suitable semiconductors like,
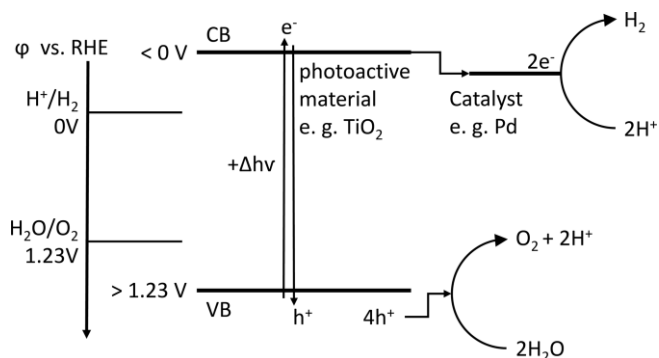

Figure 1. Schematic mechanism of photocatalytic water splitting using a photoactive water oxidation catalyst and a co-catalyst for hydrogen evolution.

e.g., main group and/or transition metal oxides. But only a few of these materials are useful for catalytic water oxidation and proton reduction, and they are mainly used for light absorption. In order to drive the chemical reactions, co-catalysts are deposited on the surface of the semiconductors (Figure 1). Such co-catalysts can reduce the activation energy of the reactions, serve as reaction sites, facilitate charge separation and charge transport.[1]

$$2\ H^+ + D^{2-} \longrightarrow H_2 + D \tag{1}$$

with D^{2-} being an electron donor.

When using H$_2$O, the electron donor would be O^{2-}, producing O$_2$ by oxidation according to Equation (2).

$$2\ H_2O \longrightarrow 2\ H_2 + O_2 \qquad \Delta G^0 = 1.23\ eV \tag{2}$$
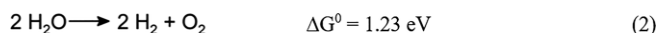
But this reaction needs high oxidation potentials, is energetically demanding and kinetically challenging.[1,2] Since both gases are produced in an identical environment, the back reaction may occur and water is formed.[16] Additionally, the oxygen

[a] Dr. M. Poschmann, Prof. Dr. W. Bensch
     Institute of Inorganic Chemistry, Kiel University,
     Max-Eyth Straße 2, 24118 Kiel, Germany
     E-mail: wbensch@ac.uni-kiel.de
     http://www.ac.uni-kiel.de/de/bensch/startseite
[b] H. Groß, T. Dankwort, Prof. Dr. L. Kienle
     Institute of Materials Science, Kiel University,
     Kaiserstraße 2, 24143 Kiel, Germany
[c] R. Amin
     Department of Chemistry, Faculty of Sciences, University of Guilan,
   P.O. Box 41335-1914, Rasht, Guilan, Iran
[d] C. Fritsch, H. Radinger, Dr. S. Indris
     Institute for Applied Materials, Karlsruhe Institute of Technology (KIT),
     Hermann-von-Helmholtz-Platz 1, 76344 Eggenstein-Leopoldshafen,
     Germany

EurJIC
European Journal of Inorganic Chemistry

Full Paper
doi.org/10.1002/ejic.202000555

Chemistry
Europe
European Chemical
Societies Publishing

produced is economically of no relevance, and more useful electron donors may be organic substances which are chemically modified (oxidized) in the hydrogen evolution reaction (HER) thus leading to formation of useful organic products.[17,18]

A widely applied electron donor is triethanolamine (TEOA), which is first oxidized to its radical cation which then decomposes via hydrolysis to glycoaldehyde and diethanolamine (Scheme 1).[19–22]
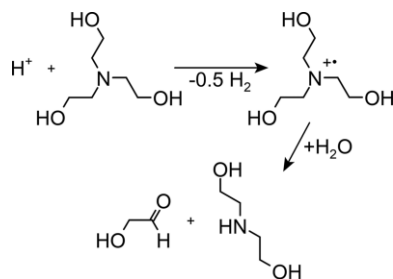
Scheme 1. Reaction pathways of oxidation of TEOA.

One of the most prominent material used in photocatalytic hydrogen production is TiO_2, exhibiting a crystal structure-dependent band gap of 3 - 3.2 eV,[1,23–25] and good stability in aqueous media. In addition, the energy positions of the valence band (VB, 2.6 - 2.7 V vs. RHE) and the conduction band (CB, −0.67 to −0.9 V vs. RHE) are suitable for H_2O/HO^- oxidation (oxygen evolution reaction, OER) and proton reduction, respectively. In addition, a mixture of rutile and anatase phases is most promising because charge carriers excited in anatase (indirect band gap, E_g = ca. 3.2 eV)[1] can be accumulated in rutile (direct band gap E_g = 3.0 eV).[1] Despite being a direct band gap semiconductor, rutile seems to exhibit a longer life time for electron-hole pairs than anatase.[26] Additionally, rutile shows higher catalytic activity for OER, while anatase has higher activity for HER if co-catalysts are applied.[27] TiO_2 itself is a poor catalyst for HER, while using e.g. Pt or Pd as co-catalysts yields very active materials[28–31] which are often used as benchmarks for comparison with different catalytic systems and setups.[1,32] Because the noble metals Pd and Pt are precious and costly, an intense search is going on to replace these metals by cheaper and more abundant materials. Materials fulfilling these needs and exhibiting high catalytic activities are transition metal sulfides like

MoS_2,[33,34] WS_2,[34,35] NiS_x,[36–38] CuS[39–41] or CoS_x.[42] All of them show synergistic effects when combined with semiconductors like TiO_2.[33–43] These binary sulfides are semiconductors with a small band gap and the combination with TiO_2 can be regarded as a Z-scheme catalyst system. Metallic transition metal sulfides may be suitable candidates for replacing noble metals as co-catalysts. A promising material is metallic $CuCo_2S_4$, crystallizing in the cubic spinel structure (space group Fd-3m).[44] Co atoms occupy 1/2 of the octahedral sites and Cu atoms are located in 1/8 of the tetrahedral sites of a closed packed topology of S atoms.[44] Charge neutrality of the compound was intensively investigated in the past and led to different oxidation state assignments like $Cu^{1.2}(Co_2)^{4.8}(S_4)^{-VI}$,[45] $Cu^{II}Co^{III}_2(S_4)^{-VIII}$,[46–49] $Cu^{I}Co^{III}_2(S_4)^{-VII}$.[44,50] We are aware that in several contributions $CuCo_2S_4$ was identified as a semiconductor with band-gaps of 2.24 eV,[51] 1.01–1.4 eV[52] or 1.41 eV.[53]

The high electrical conductivity[44,46,54] is beneficial for a good and fast electron transfer to surface sites, being able to use excited electrons for catalytic reactions. In some studies, $CuCo_2S_4$ showed excellent activity for electrochemical HER and OER making it a bifunctional catalyst for water splitting and a very interesting material for further investigations.[55–57]

We used $CuCo_2S_4$ as a co-catalyst deposited in varies amounts on TiO_2 (P25®) and observed a strong concentration dependence of the photocatalytic activity of the composites for HER. We investigated the influence of the pH value on the HER activity and the long-term stability. Variation of the pH value led to a significant improvement of the HER and an enormous long-term stability. Here we report the results of the investigations together with the characterization of the materials.

Results and Discussion

X-ray Powder Diffraction

Because the good electrical conductivity of $CuCo_2S_4$ is accompanied by a high light absorptivity and reflectivity, the amount of $CuCo_2S_4$ on TiO_2 was adjusted to low percentages. Hence, three different samples were solvothermally prepared with nominally 5, 10 and 20 wt.-% of the spinel (abbreviated as CCS5, CCS10 and CCS20). The X-ray powder pattern of CCS10 shows reflections of anatase and rutile (see Figure 2 and Supporting Information Figure S6 and S7 for CCS5 and CCS20), together

Table 1. Selected structural data obtained by Rietveld refinements of XRD data of the sample CCS10. Estimated standard deviations are given in parentheses.

Parameter	Anatase	Rutile	$CuCo_2S_4$
Cell parameter [Å]	a = b = 3.78646(3)	a = b = 4.59480(10)	a = b = c = 9.4701(4)
	(3.7842(13)[59])	(4.595(1)[59])	(9.478(5)[63])
	c = 9.50690(12)	c = 2.95970(13)	
	(9.5146(15)[59])	(2.959(1)[59])	
Chalcogen position	x = y = 0	x = y = 0.30479	x = y = z = 0.263
	z = 0.20732	(0.30479(10)[62])	(0.263[63])
	(0.2081(2)[61])	z = 0	
Space group	$I4_1/amdS$	$P4_2/m$ nm	Fd-3mZ
R-Bragg	0.910	1.784	1.257
Weight fraction [%]	82.0	11.5	6.0
Volume-averaged domain size [nm]	23	33	14

with reflections of $CuCo_2S_4$ exhibiting a relatively low intensity. Results of the Rietveld refinement of CCS10 (Table 1; Table S2 for CCS5 and CCS20) yield ≈ 82 wt.-% anatase, ≈ 12 wt.-% rutile and ≈ 6 wt.-% $CuCo_2S_4$. Because P25® may contain 8–13 wt.-% of amorphous titania,[58–60] the wt.-% of $CuCo_2S_4$ has to be regarded as an estimate. The unit cell parameters of anatase, rutile and $CuCo_2S_4$ are in the range reported in literature (see Table 1).[61–63] The volume-weighted mean diameter of the coherently-scattering domains was estimated from the integral breadth of the Bragg reflections (shape factor: 0.89 for spherical crystallites). For anatase and rutile, the volume averaged domain diameters are 23 and 32 nm, respectively. Both values are in the range reported in literature where fluctuations in composition and domain diameters were reported.[58–60] For $CuCo_2S_4$, an isotropic domain diameter of 14 nm is obtained (data for CCS5 and CCS20 see Supporting Information Table S2).
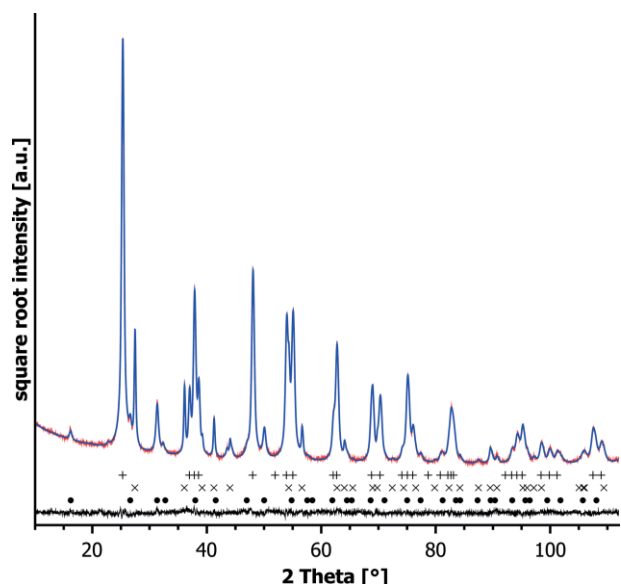

Figure 2. Rietveld refinement data of CCS10. Measured data (red), simulated data (blue), and difference curve (black). Marks correspond to reflection positions of anatase[61] (+), rutile[62] (x) and $CuCo_2S_4$[63] (●). The difference curve shows that the experimental and simulated patterns match perfectly.

Transmission and Scanning Electron Microscopy

Transmission electron micrographs of the samples show the presence of large agglomerates on a micrometer length scale, consisting of nano-crystallites. From HRTEM micrographs, *d*-values of the crystallites were obtained which allow differentiation between different phases. Accordingly, rutile and anatase crystallites could be identified (Figure 3a and Supporting Information Figure S5). Further, HRTEM micrographs and corresponding FFT (zone axis [112]) verify the presence of $CuCo_2S_4$ crystallites. The polydisperse crystallites exhibit diameters of 10 nm to 40 nm and the results are in good agreement with XRD data. The nano-crystallites do not exhibit prominent crystal defects like intergrown domains or shear structures.
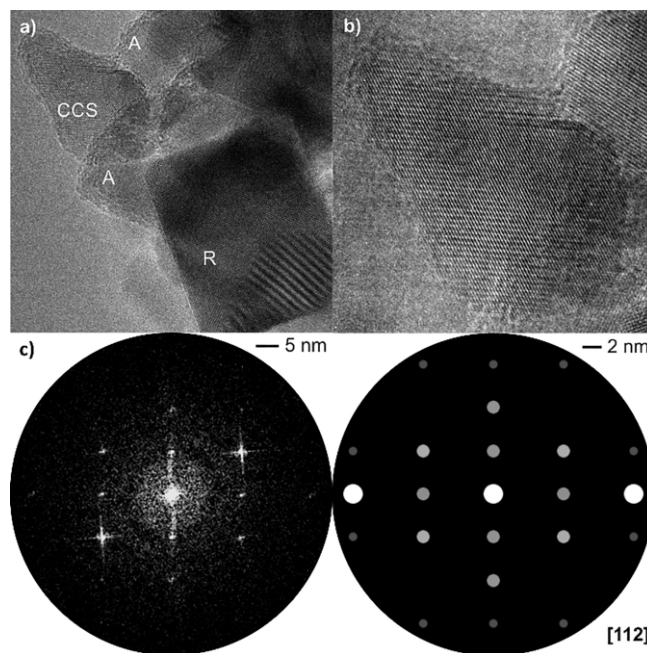

Figure 3. Transmission electron micrographs and electron diffraction patterns of a particle cluster of CCS10. (a) Overview micrograph showing the occurrence of crystallites whose d-spacings could be attributed to anatase (A),[61] rutile (R),[62] and $CuCo_2S_4$ (CCS).[63] (b) HRTEM micrograph of the $CuCo_2S_4$ crystallite found in (a). (c) Corresponding FFT and simulated diffraction pattern of $CuCo_2S_4$ in zone axis [112], showing good agreement. Differences in intensity may occur due to misalignment of the crystallite and the impact of the contrast transfer function on the peak intensity of FFT.

Diffuse Reflectance Spectroscopy

The diffuse reflectance data is transformed into absorption data via the Kubelka-Munk function using Equation (3).

$$\alpha = \frac{(1 - R_\infty)^2}{2R_\infty} \tag{3}$$

with the Kubelka-Munk absorptivity α and $R\infty$ as relative diffuse reflectivity calculated by Equation (4).

$$R_\infty = \frac{R_{Sample}}{R_{Standard}} \tag{4}$$

with the reflectivity of the sample R_{Sample} and the reflectivity of the pure white standard $R_{Standard}$, in this case NaCl.[64]

The Kubelka-Munk curve of CCS10 (Figure 4) shows a very broad diffuse photon absorption in the higher wavelength range from 390 to 2000 nm. For CCS5, the absorptivity is less intense, while for CCS20, the absorptivity is increased due to higher loading of $CuCo_2S_4$ compared to CCS10 (see Supporting Information Figure S8). For pure $CuCo_2S_4$ no distinct light absorption edge between 300 and 1800 nm is observed excluding semiconducting behavior of the material (see Supporting Information Figure S10). This explains the greyish black color of the samples and is a result of metallic character of $CuCo_2S_4$.[44,46] At higher energies, a strong increase of the absorptivity is observed due to the absorption edge of rutile.[1] A Tauc-plot (see Figure 4) gives a linear dependency of the band edge[65] of 3.3 eV (365 nm), which is similar to values reported for rutile in P25® (3.35 eV).[60] The band gap of anatase could not be deter-

EurJIC
European Journal of Inorganic Chemistry

Full Paper
doi.org/10.1002/ejic.202000555

Chemistry Europe
European Chemical
Societies Publishing

mined because it is not possible to accurately determine additionally an indirect band gap at higher energies due to the low absorptivity. The photon absorptivity of TiO_2 materials in CCS5 and CCS20 is similar to that of CCS10 (see Supporting Information Figure S9). All samples show an absorption edge at 365 nm (3.3 eV) in the diffuse reflectance spectra originating from TiO_2 within the composites.
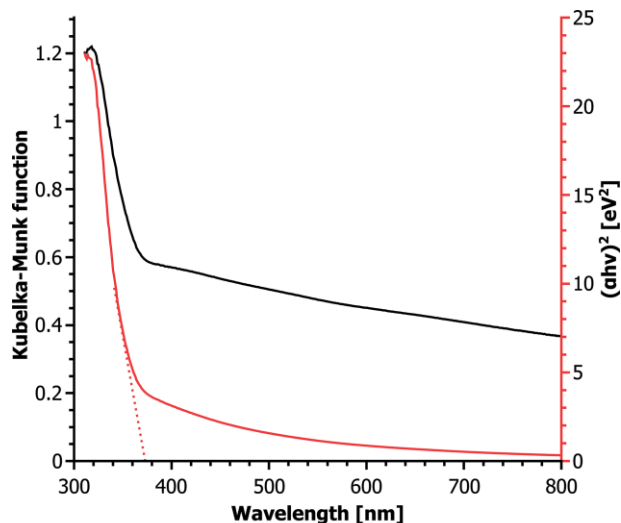

Figure 4. Kubelka-Munk term (black) and Tauc-plot (red) calculated from the observed diffuse reflectivity data of CCS10 showing the broad absorption of $CuCo_2S_4$ at higher wavelengths and the absorption edge of TiO_2 at high energies (dotted line).

Nitrogen Sorption Experiments

The N_2 sorption data of CCS5, CCS10 and CCS20 show type II isotherms, a typical dependency for nonporous or macroporous materials having no limitation of multilayer adsorption (see Figure 5).[66] The BET analysis[67] (see Supporting Information Figure S2) yields a specific surface area of 40 m²/g, 39 m²/g and
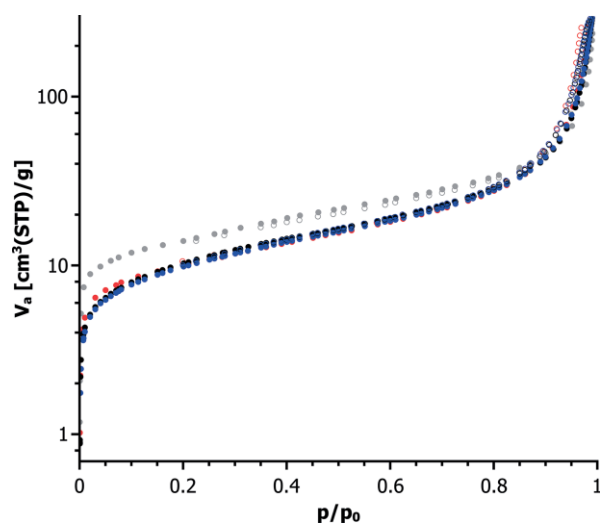
38 m²/g for CCS5, CCS10 and CCS20, respectively. Compared to pure P25® (49 m²/g), the specific surface area is reduced by ca. 26 % which may be explained by the deposition of $CuCo_2S_4$ on TiO_2 particles increasing the particle diameter and weight while not increasing the surface area. Therefore, the amount of $CuCo_2S_4$ seems to have only a weak influence on the specific surface area.

Photocatalytic Experiments

At the beginning of the photocatalytic measurement, the evolution of a discrete gas volume is related to light induced heating of the reaction mixture. Afterwards, a very pronounced gas volume evolution of 0.8 mL/h is observed for more than 9.5 h (see Figure 6) due to H_2 generation as evidenced by gas chromatographic analysis. Assuming an ideal gas, the amount of H_2 is 33.6 μmol/h for CCS10. This value is only about 2.8 times lower than the H_2 production of P25®@Pd 1 wt.-% (94.6 μmol/h), see Table 2 and Supporting Information Figure S15), but comparable to reported activities for similar TiO_2@Pd catalysts.[30,31,68] As mentioned above, TiO_2 exhibits only very low photocatalytic activity for HER which is explained by fast recombination of electrons and holes, a pronounced back reaction, and a large overpotential at the surface for H_2 production. Hence, the high catalytic activity of CCS10 is caused by a synergistic effect. The catalyst loading of 10 wt.-% seems to be almost ideal because of the significantly higher activity compared to the other two catalysts (see Table 2 and Figure 6). For CCS5, no catalytic activity is observed, most probably caused by the low loading with $CuCo_2S_4$ preventing generation of a synergy with TiO_2. Using CCS20, an H_2 evolution rate of 24.8 μmol/h is obtained, which is about 25 % lower than for CCS10. The observation of an optimal loading is not unusual and possible explanations are a decreased absorption of light by TiO_2, the introduction of more recombination centers and/or a decrease of the number of ac-

Figure 5. Detected N_2 sorption data of P25® (gray), CCS5 (black), CCS10 (red) and CCS20 (blue) showing typical characteristics of a nonporous material.
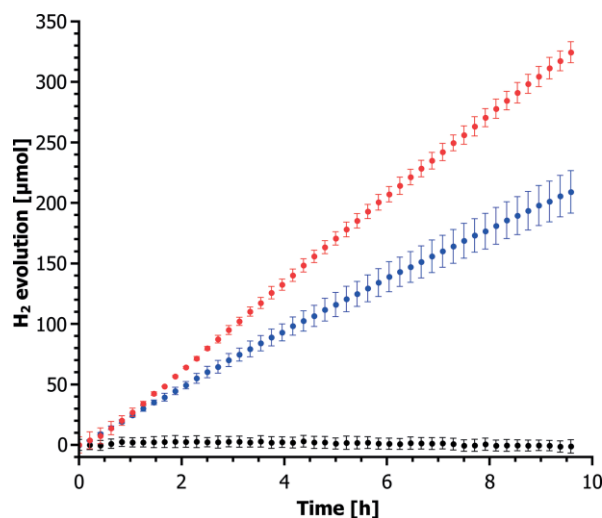

Figure 6. Mean hydrogen evolution observed during irradiation of CCS5 (black), CCS10 (red) and CCS20 (blue) dispersed in 10 vol.-% aqueous TEOA solution. Error bars represent the standard deviation estimated from different measurements.

Table 2. Photocatalytic hydrogen evolution rates compared to data of metallic co-catalysts reported in literature for selected similar systems, using 300 W Xe lamp irradiation and triethanolamine as sacrificial agent.

Sample	Low pass light filter [nm]	Sacrificial agent used in aqueous solution	Hydrogen evolution rate [μmol/h]
$(Cu,In)_{0.2}Zn_{1.6}S_2$@Pt[80]	420	10 vol.-% TEOA	17.5
TiO_2@Rh + y-Eosin[81]	420[c]	15 vol.-%	15.3
TiO_2@Ru + y-Eosin[81]	420[c]	15 vol.-%	12.3
TiO_2@Pt + y-Eosin[81]	420[c]	15 vol.-%	5.7
TiO_2@Cu + y-Eosin[82]	420	10 vol.-%	1330[d]
TiO_2@MWCNT@Pt[83]	420	15 vol.-% TEOA	15.1
TiO_2[84]	420	20 vol.-% TEOA	0.36
P25®@Pd	320	10 vol.-% TEOA	94.6[a]
CCS5	320	10 vol.-% TEOA	traces
CCS10	320	10 vol.-% TEOA	33.6[a]
			28.0[b]
CCS20	320	10 vol.-% TEOA	24.8[a]
			8.4[b]
P25®	320	10 vol.-% TEOA	traces
$CuCo_2S_4$	320	10 vol.-% TEOA	traces
P25® and $CuCo_2S_4$	320	10 vol.-% TEOA	26.4[a,b]
P25® with Cu^{II}/Co^{II}-chloride	320	10 vol.-% TEOA	traces

[a] Estimated standard deviations calculated from different measurements are between 3 and 8 %. Note for the Pd sample the value is slightly larger. [b] Evolution rate given in mmol/($g_{CuCo2S4}$ h). [c] 200 W halogen lamp. [d] Evolution rate given in μmol/(g h), unfortunately the amount of catalyst used was not reported.

tive sites on the TiO_2 surface, an incomplete dispersion of the particles on the surface, and increased particles sizes.[69]

We note that H_2 evolution in the present system is not forced or enhanced by hot electron injection from $CuCo_2S_4$ on TiO_2 like observed for Au@TiO_2.[70–72] In $CuCo_2S_4$, the dominant charge carriers are holes.[45,54] These can possibly be excited by plasmon resonance and injected as ›hot holes‹ into neighboring materials. But TiO_2 is an electron acceptor and acts as a hole donor.[72,73] Therefore, neither hot electron nor hot hole injection from $CuCo_2S_4$ to TiO_2 is likely.

A comparison of the catalytic activity of materials is not straightforward due to the differing experimental setups, the different numbers reported for the activity, and the sacrificial agents applied. The effect of the latter was recently summarized in a review, showing that the catalytic activity of pure P25® strongly depends on the sacrificial agents.[74] The highest activity was observed for TiO_2/ethylene glycol (190.2 μmol H_2 in 6 h) and the lowest for lactic acid (27.6 μmol in 6 h), while TiO_2/TEOA produced a low amount of 61.8 μmol H_2 in 6 h. Keeping all the difficulties in mind, we compare the performances of selected catalytic systems in Table 2 to give the reader an impression about the activity of CCS10. As can be seen from the data, CCS10 and CCS20 show a far higher activity for H_2 evolution compared to other catalysts under comparable conditions (300 W Xe arc lamp and triethanolamine as sacrificial agent). Especially, the higher activity compared to metallic co-catalysts like Cu, Pt, Ru or Rh reveals that $CuCo_2S_4$ is a promising co-catalyst for photocatalytic hydrogen evolution. It should be noted that effects of the different light filters used in literature cannot be easily taken into account. For example, the utilizable photon energy using sensitizers like y-Eosin is smaller than that of TiO_2. Therefore, the used light filter has a large effect on the photocatalytic activity and the number of photons has to be considered for better comparability.

Chemical actinometry with $K_3Fe(C_2O_4)_3$·$3H_2O$ gave a value for the photon flux of 5.4 ± 0.4 μmol/s for the 300 W Xe arc lamp, when applying a 320 nm low pass filter in the relevant wavelength range from 250 to 500 nm. Using the formula [Equation (5)] below:

$$PE\,(250-500\,nm) = \frac{2 \cdot R^{in}}{R_{O,250-500\,nm}} \qquad (5)$$

the photonic efficiency (*PE*) can be calculated, with the initial H_2 production rate R^{in} and photon flux $R_{O,250-500\,nm}$ determined by the actinometry system.[8,75–79] The photonic efficiency of CCS10 is 0.35 ± 0.02 %, while P25®@Pd 1 wt.-%, which was tested for comparison, reached a value of 0.98 ± 0.14 %. A much larger efficiency cannot be expected because the majority of the photons (see Supporting Information Figure S3) has no sufficient energy to generate electron-hole pairs in TiO_2. For the catalyst with higher loading, the photonic efficiency is 0.26 ± 0.02 %.

The H_2 evolution rate of CCS10 decreases slowly with time, which may be explained by an increasing shortage of the sacrificial agent or due to deactivation of the catalyst. After the first catalytic test, the catalyst was reused in a second test and after this run, the material was recovered for a third test (see Figure 7). The experiments show that the activity of the catalyst is slowly decreasing over time during the very long irradiation time of 70 to 80 h, but still ca. 1.2 mmol H_2 were produced. Assuming a linear decrease of H_2 evolution rate, the half-life time of activity is ca. 42 h. We note that in many studies irradiation of the catalytic system is restricted to only a few hours, which does not allow judgement of the stability.

The synergism in photocatalytic activity of $CuCo_2S_4$ and TiO_2 becomes apparent when using pure P25®, $CuCo_2S_4$ or a mechanical mixture of both materials (for characterization of these materials see Supporting Information Figure S11, S12, and Table

EurJIC
European Journal of Inorganic Chemistry

Full Paper
doi.org/10.1002/ejic.202000555

Chemistry Europe
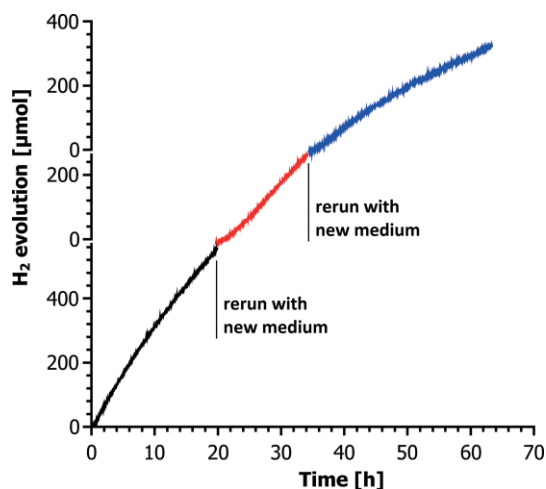European Chemical Societies Publishing

Figure 7. H$_2$ evolution using CCS10 as photocatalyst in aqueous TEOA solution for the first (black), second (red) and third (blue) time with new reaction medium each time showing the slowly decreasing activity with time.

S5). Pure P25® or CuCo$_2$S$_4$ show no sufficient ability for photocatalytic H$_2$ evolution under the conditions applied in the experiments (see Supporting Information Figure S13), and only traces of H$_2$ could be detected. A mechanical mixture of 10 wt.-% CuCo$_2$S$_4$ in P25® shows a lower H$_2$ evolution rate (26.4 mmol/(g$_{CuCo2S4}$ h)) compared to CSS10 (28.0 mmol/(g$_{CuCo2S4}$ h)) based on the CuCo$_2$S$_4$ content determined by XRD. Additionally, the half-life time of H$_2$ evolution rate with the mechanical mixture (21 h) is lower than CCS10. These results indicate a better interaction and connection of TiO$_2$ and CuCo$_2$S$_4$ in CCS10 compared to the mechanical mixture.

Post Catalytic Characterization

The XRD pattern of CCS10 after the catalytic test shows a reduced intensity of the reflections of CuCo$_2$S$_4$ compared to the pattern of the pristine material (see Figure 8). This observation indicates either an amorphization of CuCo$_2$S$_4$, a dissolution or a detachment of the spinel particles from the TiO$_2$ surface. Chemical analyses of the recovered CuCo$_2$S$_4$/TiO$_2$ nanocomposites revealed a decrease of the Cu, Co and S content with increasing irradiation time. After 80 h of irradiation, Cu vanished and only 1.1 ± 0.2 wt.-% of Co could be detected via EDX on the catalyst material (see Supporting Information Table S1). One may speculate that dissolution and oxidation of S^{2-} ions are responsible for the H$_2$ evolution. However, this would only account for a maximum H$_2$ evolution of 0.2 mmol, which is much less than the value obtained after 80 h irradiation time (compare Figure 7). To gain insight into the catalyst deactivation, CCS10 was stirred in the dark for 20 h under the same conditions as photocatalytic measurements and EDX data were collected. Indeed, the amount of Cu, Co, and S was reduced, which indicates slow dissolution of the spinel material. In the basic aqueous TEOA solution, traces of Cu^{2+} and Co^{2+} ions could be detected (see Supporting Information Figure S4). These results demonstrate that the presence of OH$^-$ ions is responsible for the catalyst deactivation. Hence, the effect of OH$^-$ concentra-

tion on the catalytic activity and stability must be identified which is discussed below. To demonstrate that dissolved metal ions are not the active catalysts, photocatalytic experiments with P25® and dissolved Cu^{II} and Co^{II}-salts were done under similar conditions (see Supporting Information Figure S14). In these experiments, no hydrogen evolution could be observed like using pure P25®. This finding is a clear evidence that Cu-Co$_2$S$_4$ is the active co-catalyst.
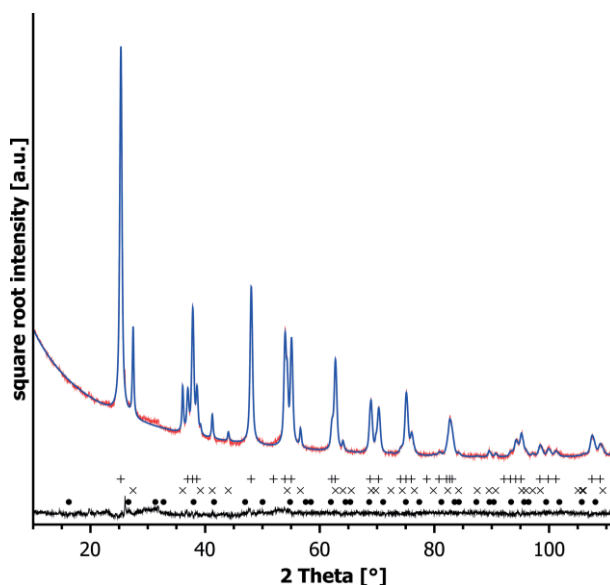

Figure 8. Rietveld refinement data of CCS10 after usage in a catalysis experiment with 20 h irradiation. Measured data (red), simulated data (blue), and difference curve (black). Marks correspond to reflection positions of anatase[61] (+), rutile[62] (x), CuCo$_2$S$_4$[63] (*). Intensity of reflections of CuCo$_2$S$_4$ are explicitly lowered compared to the as synthesized material.

Mass Spectrometry of the Solvent

Analysis with electro spray ionization mass spectrometry (ESI-MS) of the organic components in solution after catalysis showed no presence of oxidation products of TEOA. Using molecular catalysts like tris-(2,2′-bipyridine)-Ru(II)-chloride results in the formation of diethanolamine and glycoaldehyde as oxidation products.[22] In contrast, CuCo$_2$S$_4$ deposited on TiO$_2$ offers free coordination sites and TEOA molecules possibly coordinate to these sites being fully oxidized without releasing diethanolamine and/or glycoaldehyde.

Impedance Measurements of CCS10

Temperature dependent Nyquist plots (see Supporting Information Figure S19 and given fitting details) show a typical shape of frequency-dependent resistivity similar to comparable materials.[85,86] At 30 °C, the temperature used for photocatalytic experiments, the estimated materials conductivity amounts to ca. 2.15 µS/cm.

EurJIC
European Journal of Inorganic Chemistry

Full Paper
doi.org/10.1002/ejic.202000555

Chemistry Europe
European Chemical
Societies Publishing

Via the relation [Equation (6)],

$$\sigma = \sigma_0 \cdot e^{\left(-\frac{E_a}{k_B T}\right)} \tag{6}$$

(σ = materials conductivity, σ_0 = prefactor, k_B = Boltzmann constant,
T = temperature, E_a = activation energy)

an Arrhenius plot (see Supporting Information Figure S19) allows an estimation of the activation energy E_a necessary for obtaining electrical conductivity in the material, being 0.42 eV (41 kJ/mol). This is ten times higher than the value found for anatase single crystals[87] and 3 to 7 times higher than observed for polycrystalline samples.[88–90] Reasons are possible a looser packing of crystallites in the pelletized sample or a different mean crystallite size. Thus, density and type of dopants, surrounding atmosphere, UV-irradiation and anatase/rutile ratio will as well affect the materials conductivity and activation energy.[91,92]

With the potential-dependent capacitance data, a Mott-Schottky diagram is constructed to extract the flat-band potential of the conduction band of the material (see Figure 9). Since the occurring linear slope is positive, the material is an n-type semiconductor.[87,93,94] The flat band potential of CCS10 occurs at −0.21 V vs. RHE. This is in the range of flat-band potentials observed for pure P25® (E_{FB} = -0.67 V vs. RHE at pH = 7,[93] E_{FB} = −0.211 V vs. RHE at pH = 7[94]), suggesting that $CuCo_2S_4$ on the surface of TiO_2 does not influence the electronic characteristics of TiO_2.

to 55.9 μmol/h (see Figure 10, Table 3 and Supporting Information Figure S15). Further decrease of the pH value led to a drop of the photocatalytic activity to 32.3 μmol/h and 3.8 μmol/h at pH values of 7.2 and 1.4, respectively. This is the result of protonation of TEOA molecules losing the surface coordination ability at pH values lower than the pK_a value (7.74[95]). Thus, photocatalytic activity is highest under mild basic conditions. In addition, a lower pH value reduces the solubility of Cu based sulfides,[96–99] resulting in a higher stability and better long-term stability of the catalyst. This can be seen in XRD patterns of CCS10 obtained after catalysis runs of 20 h at different pH values (see Supporting Information Figure S16), with the best results being obtained at pH = 7.2 in a long-term experiment. The total irradiation time was 70 h with an intermediate stop after 45 h and a restart with fresh TEOA solution (see Supporting Information Figure S17). During this time, the huge total amount of 2 mmol H_2 was produced. The H_2 evolution of each step can be fitted linearly with R^2 values of ca. 0.999, indicating long-term stability of CCS10 at this pH value. The slightly lower H_2 evolution rate in the second run compared to the first one originates from the catalyst recovery process. The long-term stability of CCS10 is comparable to that of Pt/TiO_2,[100] Rh/TiO_2,[81] Pd/TiO_2,[31] CuS/TiO_2,[40,41] CoS_x/TiO_2,[43] TiO_2@MoS_2@CdS,[101] MoS_2/CdS,[102] TiO_2@MoS_2[103] and Pt/TiO_2/C_3N_4[104] for which H_2 production was investigated between 20 and 50 h.
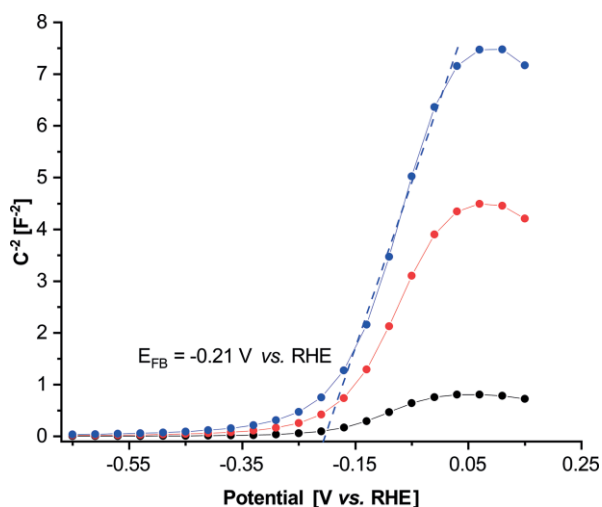

Figure 9. Mott-Schottky plot of CCS10 measured at frequencies of 103 Hz (black), 522 Hz (red) and 1046 Hz (blue). Linear interpolation of the linear region to the abscissa yields the flat-band potential of the conduction band E_{FB} of −0.21 V vs. RHE.
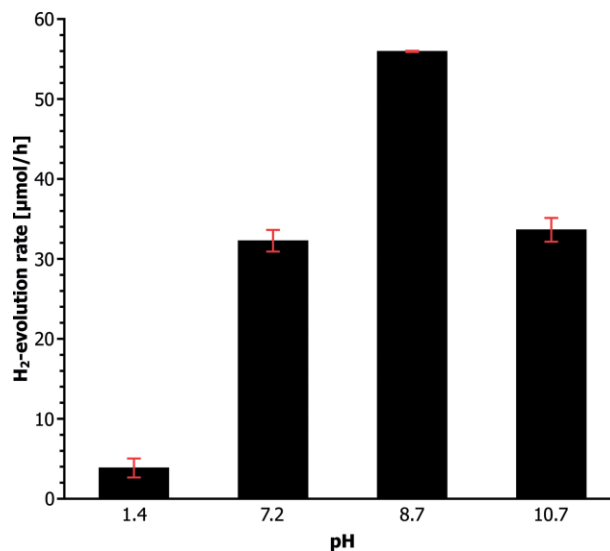

Figure 10. Initial hydrogen evolution rates with standard deviations observed for CCS10 at different pH values.

pH Value and Wavelength Dependency of Catalytic Activity

The influence of pH value on the catalyst performance was monitored by adjusting the pH of the TEOA solution, small amounts of conc. H_2SO_4 were added, while the photocatalytic measurements were done as described above.

The pH value of the pure 10 vol.-% TEOA solution is 10.7. Decreasing the pH to 8.7, the photocatalytic activity increases

The photocatalytic activity of $CuCo_2S_4$ on TiO_2 is strongly wavelength-dependent, because electrons in TiO_2 can only be excited with light of wavelength ≤ 365 nm (see Figure 4). If a ≥ 420 nm low pass cut-off light filter is used, instead of the ≥ 320 nm filter, no H_2 evolution is observed (see Table 3 and Supporting Information Figure S18). This result strongly confirms that $CuCo_2S_4$ is not being photoactive in the present system. Photons are absorbed by TiO_2 generating electron-hole pairs and electrons are transferred to $CuCo_2S_4$ that is responsible for the reduction of protons.

EurJIC
European Journal of Inorganic Chemistry

Full Paper
doi.org/10.1002/ejic.202000555

Chemistry Europe
European Chemical
Societies Publishing

Table 3. Observed photocatalytic H_2 evolution rates and photonic efficiencies at different pH values of reaction medium.

pH value	Irradiation wavelength	H_2 evolution rate [µmol/h]	Photonic efficiency [%]
1.4	≥ 320 nm	3.8	0.04
7.2	≥ 320 nm	32.3	0.33
7.2	≥ 420 nm	Not detectable	
8.7	≥ 320 nm	55.9	0.58
10.7	≥ 320 nm	33.6	0.35

Conclusions

Using a solvothermal approach, metallic $CuCo_2S_4$ nanoparticles were deposited on TiO_2 nanocrystals consisting of a mixture of rutile and anatase. The accessible specific surface area was not significantly affected by the deposition of the spinel particles on TiO_2. Depending on the amount of $CuCo_2S_4$ on TiO_2, photocatalytic measurements show high catalytic activities using TEOA as sacrificial agent. The rate constant of H_2 evolution with catalyst loading of nominal 10 wt.-% reached 33.6 µmol/h corresponding to 0.8 mL/h with a photonic efficiency of 0.35 ± 0.02 %. If the loading of $CuCo_2S_4$ on TiO_2 is too low or too high, the catalytic performance is much lower. Adjusting the pH value to nearly neutral values increases the long-term catalytic performance drastically. At pH = 7.2, a H_2 evolution of 2 mmol is observed for a long period of 70 h. The catalytic activity of CSS10 is only 2.8 times lower than that of Pd as a co-catalyst. But Pd (34000 US-$/kg)[105] is far more expensive than Co (55.5 US-$/kg),[106] which is the most expensive element in $CuCo_2S_4$. Therefore, the use of $CuCo_2S_4$ instead of Pd is very promising. In summary, a schematic mechanism can be suggested as shown in Figure 11. Electron-hole pairs are generated by light absorption by TiO_2. The electrons are transferred to the co-catalyst $CuCo_2S_4$ and H^+ ions are readily reduced to H_2. The valence band holes are filled by electrons due to oxidation of TEOA.
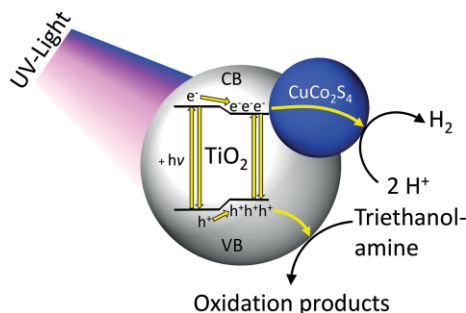

Figure 11. Schematic representation of the suggested mechanism of hydrogen evolution with P25®@$CuCo_2S_4$ in aqueous triethanolamine solution.

Experimental Section

Chemicals

$CoCl_2\cdot6H_2O$ (> 98 %, Fluka), $CuCl_2\cdot2H_2O$ (≥ 99 %, Merck), P25® (TiO_2, 99.5 %, Degussa), thiourea (≥ 98 %, Merck), triethanolamine (TEOA, ≥ 99 %, Fluka), $FeCl_3\cdot6H_2O$ (> 98 %, Sigma Aldrich), $K_2C_2O_4\cdot H_2O$ (99 %, Merck), K_2PdCl_4 (> 98 %, Degussa), H_2SO_4 (96 %, Walter CMP), acetone (97 %, Walter CMP), ammonium acetate (≥ 98 %, Fluka), Ethanol (99 %, methylated, Walter CMP), 1,10-phenanthroline (99 %,

ABCR), NaCl (> 99.5 %, Grüssing) were used without further purification.

Synthesis of Photocatalysts

The synthetic procedure for P25®@$CuCo_2S_4$ 10 wt.-% (CCS10) is related to that reported by Qizhao et al. and was as follows.[107] 340 mg of P25® was stirred for 1 h in 10 mL of deionized water. Then, 18.8 mg (0.11 mmol) of $CuCl_2\cdot2H_2O$, 52.4 mg (0.22 mmol) of $CoCl_2\cdot6H_2O$ and 50 mg (0.66 mmol) thiourea dissolved in 3 mL deionized water and 2 mL conc. aqueous ammonia were added and the slurry was stirred for 1 h. The resulting dispersion was sonicated for 0.5 h and then transferred into a Teflon®-lined steel autoclave with a total volume of 30 mL. The sealed autoclaves were then heated to 180 °C for 12 h. Afterwards the formed solid was filtered and washed multiple times with demineralized water and ethanol and dried in air at ambient temperature. Greyish black powders were obtained (yield ca. 67 %). After characterization of the samples with EDX and XRD, individual batches were combined for further usage.

Samples with higher and lower loading of $CuCo_2S_4$ were synthesized in a similar way but using the half or double amount of Cu, Co and S sources. These samples are denoted as CCS5 and CCS20. Pure $CuCo_2S_4$ was prepared by using the same procedure as for CCS10 but without P25®. Pure $CuCo_2S_4$ was prepared by using 10-times the amount of Cu, Co and S sources without the addition of TiO_2.

For comparison a sample P25®@Pd 1 wt.-% was prepared as follows.[32] 15 mg of K_2PdCl_4 were dissolved in 5 mL demineralized water and 45 mL ethanol. 500 mg P25® are added and the mixture was stirred until a good dispersion was obtained. Then, the dispersion was stirred and irradiated for 2 h with a 300 W Xe lamp in a round-bottomed flask equipped with a cooling jacket, keeping the temperature constant at 30 °C. Afterwards, the material was separated by centrifugation, washed with demineralized water and ethanol, and then dried at 90 °C in an oven. Characterization of this material is presented in the Supporting Information (see Supporting Information Chap. S1).

Characterization

X-ray powder patterns (XRD) of all samples were recorded with a PANalytical Empyrean MPD diffractometer with Cu $K_{\alpha1,2}$ irradiation in reflection geometry. The profile function of the instrument was determined using LaB_6 SRM 660c NIST standard. Rietveld refinements of the patterns were done using the program TOPAS Academic v6[108] in combination with coding program jEdit.[109] For determination of the quantities, the linear absorption coefficients, formula weights and unit cell volumes were taken into account.

For nanostructure investigation, Transmission Electron Microscopy (TEM) was performed using a FEI Tecnai F30 G^2 STwin equipped with a field emission gun operated at 300 kV. For contrast enhancement, scripts for Gatan Digital Micrograph were used as described by Mitchell.[110] Diffraction data was simulated using the software jems.[111]

EurJIC
European Journal of Inorganic Chemistry

Full Paper
doi.org/10.1002/ejic.202000555

Chemistry Europe
European Chemical
Societies Publishing

Energy Dispersive X-ray (EDX) analyses were carried out within FEI Tecnai F30 G^2 STwin (Li:Si Detector, EDAX) or with an Environmental Scanning Electron Microscope Philips XL-30 and an Li:Si EDAX detector.

For the diffuse reflectance spectroscopy and collection of the UV/Vis spectra, the samples were ground as 1 wt.-% mixture with NaCl as white standard. The powders were measured in reflection geometry using an integrating sphere in a Varian Cary 5000 in the region 250–2000 nm. For measuring the diffuse reflectance of $CuCo_2S_4$, a mixture of 0.1 wt.-% $CuCo_2S_4$ in NaCl was used because of the deep black color of $CuCo_2S_4$.

The specific surface areas of the samples were determined with the Brunauer–Emmett–Teller (BET) method[67] using data obtained by sorption measurements with N_2 using a Belsorp Max apparatus. Before the measurements, the samples were dried in vacuo at 10^{-3} mbar at $T = 90$ °C for 16 h.

Electrochemical impedance measurements were done on CCS10 pelletized unidirectional at 100 bar (diameter = 8 mm) using a Bio-Logic SP300 instrument. The sample was contacted with Au and the measurement was done in a frequency range of 7 MHz down to 100 kHz with an amplitude of 20 mV. Mott-Schottky measurements were performed in a three-electrode electrochemical cell, using coated glassy carbon as working electrode, a graphite rod as counter counter, and Ag/AgCl (3 M KCl) as reference electrode and a pH = 4.5 phosphate buffer solution. Measurements were done in the potential range of –0.65 V to 0.15 V vs. RHE at frequencies of 1 Hz to 7 MHz with an amplitude of 10 mV. Prior to the experiment, the Ag/AgCl electrode was calibrated vs. RHE in a Phosphate buffer solution. The sample was dispersed in a 0.25 wt.-% Nafion solution (Sigma-Aldrich) before coating.

Photocatalytic Measurements

Measurements of the photocatalytic activity were undertaken with a Gasmess system of the Messen Nord GmbH. It consists of an enclosed glass tube system connected to a round-bottomed flask, a membrane pressure sensor, a vacuum pump, argon supply and an automatic syringe. The system monitors pressure increases and uses the automatic syringe to correct the pressure to the starting value to keep the setup isobar. Every part of the setup is surrounded by a cooling jacket keeping the system at a constant temperature of 30 °C applying a thermostatic water bath. In each catalytic run, 20 mg of catalyst were added into the flask. Afterwards, the gas phase was purged with Argon followed by addition of 50 mL of degassed 10 vol.-% aqueous triethanolamine (TEOA) solution. After stabilization of the pressure, a 300 W Xe arc lamp equipped with low pass ≥ 320 nm cut off filter in a distance of 15 cm was switched on to irradiate the flask (irradiated area 39.3 cm^2). The volume increase was detected vs. time. After each measurement, 10 mL of the gas phase were extracted and injected into a gas chromatograph (Agilent 6890 Plus with 5 Å molsieves column and TCD detector) to determine the hydrogen content. Errors are given as standard deviations of single measurements or as linear error propagations.

To demonstrate the synergism between P25® and $CuCo_2S_4$, additional experiments were done using pure P25®, pure $CuCo_2S_4$ and a mechanical mixture of both. In these experiments 20 mg P25® and/or 2 mg $CuCo_2S_4$ were used as catalyst. All other conditions were the same as in the experiments mentioned above.

To evaluate the influence of dissolved Cu^{II}- and/or Co^{II}-species on the photocatalytic activity of CCS5, CCS10 and CCS20, photocatalytic measurements were done using 20 mg P25®, 1 mg $CuCl_2\cdot2H_2O$ and 3 mg $CoCl_2\cdot6H_2O$, matching the amount of Cu- and Co-ions in

CCS10, as catalyst. All other conditions were identical as in experiments mentioned above.

To evaluate the influence of pH on the photocatalytic performance, TEOA solutions with different pH values were prepared by adding small amounts of conc. H_2SO_4 to the 10 vol.-% aqueous TEOA solution. The pH value was controlled with an electronic pH-meter (WTW InoLab Series pH 720). Photocatalytic experiments with these solutions were done as described above.

Actinometry

The measurement of the photon flux of the setup for photocatalytic investigations was done with the chemical actinometer system $K_3Fe(C_2O_4)_3\cdot3H_2O$ in 0.05 M H_2SO_4 solution as suggested by IUPAC for the wavelength range from 450 to 250 nm.[112] Therefore, $K_3Fe(C_2O_4)_3\cdot3H_2O$ was prepared freshly by dissolving $K_2C_2O_4$ (22.5 mmol) in water and adding a solution of $FeCl_3\cdot9H_2O$ (7.5 mmol) in the dark. After crystallization at 0 °C and after two times recrystallization from 20 mL demineralized water, large green crystals of pure $K_3Fe(C_2O_4)_3\cdot3H_2O$ were obtained (yield 78 %). For the actinometry 0.49 g of $K_3Fe(C_2O_4)_3\cdot3H_2O$ were dissolved in the dark in 50 mL of 0.05 M sulfuric acid. Every 10 seconds of irradiation, 1 mL of the solution was removed with a micropipette and added to a mixture of 1 mL 0.12 wt.-% aqueous phenanthroline solution, 1.5 mL demineralized water, 2.5 mL buffer solution (ammonium acetate 46.2 g/L and 5 mL/L sulfuric acid) and 4.5 mL 0.05 M sulfuric acid. After some hours in the dark, the UV/Vis spectra of the samples were recorded with a modular UV/Vis spectrometer consisting of a lamp (StellarNet STE-SL5-DH), probe tip with 1 cm transmission depth and spectrometer (Laser 2000 RPS-Mini-UV-CST).

Post catalytic characterization

For post-catalytic characterization, the reaction slurry containing the irradiated catalyst was added to 50 mL acetone for sedimentation of catalyst particles. The latter were separated via centrifugation at 5000 rpm and washed several times with acetone. The recovered catalysts were then characterized like the as-synthesized material using XRD, EDX and TEM. The remaining solution consisting of triethanolamine solution, acetone and possible reaction products was freed from acetone and water in vacuo with a rotary evaporator. The resulting viscous oil was examined with Mass spectrometry (JEOL AccuTOF ESI-MS).

[1] A. Kudo, Y. Miseki, *Chem. Soc. Rev.* **2009**, *38*, 253–278.
[2] X. Zou, Y. Zhang, *Chem. Soc. Rev.* **2015**, *44*, 5148–5180.
[3] T. Jafari, E. Moharreri, A. S. Amin, R. Miao, W. Song, S. L. Suib, *Molecules* **2016**, *21*, 900–928.
[4] T. Shinagawa, K. Takanabe, *ChemSusChem* **2017**, *10*, 1318–1336.
[5] S. Y. Tee, K. Y. Win, W. S. Teo, L.-D. Koh, S. Liu, C. P. Teng, M.-Y. Han, *Adv. Sci.* **2017**, *4*, 1600337.
[6] C. Acar, I. Dincer, G. F. Naterer, *Int. J. Energy Res.* **2016**, *40*, 1449–1473.

[7] Y. Miseki, K. Sayama, *Adv. Energy Mater.* **2018**, *443*, 1801294.

[8] K. Maeda, *J. Photochem. Photobiol. C* **2011**, *12*, 237–268.

[9] H. Ahmad, S. K. Kamarudin, L. J. Minggu, M. Kassim, *Renewable Sustainable Energy Rev.* **2015**, *43*, 599–610.

[10] A. J. Ragauskas, C. K. Williams, B. H. Davison, G. Britovsek, J. Cairney, C. A. Eckert, W. J. Frederick, J. P. Hallett, D. J. Leak, C. L. Liotta, J. R. Mielenz, R. Murphy, R. Templer, T. Tschaplinski, *Science* **2006**, *311*, 484–489.

[11] J. J. Bozell, G. R. Petersen, *Green Chem.* **2010**, *12*, 539–554.

[12] A. M. Appel, J. E. Bercaw, A. B. Bocarsly, H. Dobbek, D. L. DuBois, M. Dupuis, J. G. Ferry, E. Fujita, R. Hille, P. J. A. Kenis, C. A. Kerfeld, R. H. Morris, C. H. F. Peden, A. R. Portis, S. W. Ragsdale, T. B. Rauchfuss, J. N. H. Reek, L. C. Seefeldt, R. K. Thauer, G. L. Waldrop, *Chem. Rev.* **2013**, *113*, 6621–6658.

[13] R. L. Paddock, S. T. Nguyen, *J. Am. Chem. Soc.* **2001**, *123*, 11498–11499.

[14] J. K. Stolarczyk, S. Bhattacharyya, L. Polavarapu, J. Feldmann, *ACS Catal.* **2018**, *8*, 3602–3635.

[15] R. Snoeckx, A. Bogaerts, *Chem. Soc. Rev.* **2017**, *46*, 5805–5863.

[16] F. Dionigi, P. C. K. Vesborg, T. Pedersen, O. Hansen, S. Dahl, A. Xiong, K. Maeda, K. Domen, I. Chorkendorff, *J. Catal.* **2012**, *292*, 26–31.

[17] D. S. P. Cardoso, B. Šljukić, D. M. F. Santos, C. A. C. Sequeira, *Org. Process Res. Dev.* **2017**, *21*, 1213–1226.

[18] K. D. Moeller, T. Wu, B. H. Nguyen, M. C. Daugherty, *Angew. Chem. Int. Ed.* **2019**, *58*, 3562–3565; *Angew. Chem.* **2019**, *131*, 3600–3603.

[19] T. Lazarides, T. McCormick, P. Du, G. Luo, B. Lindley, R. Eisenberg, *J. Am. Chem. Soc.* **2009**, *131*, 9192–9194.

[20] M. Schwarze, D. Stellmach, M. Schröder, K. Kailasam, R. Reske, A. Thomas, R. Schomäcker, *Phys. Chem. Chem. Phys.* **2013**, *15*, 3466–3472.

[21] Z. Zhang, A. Li, S.-W. Cao, M. Bosman, S. Li, C. Xue, *Nanoscale* **2014**, *6*, 5217–5222.

[22] K. Kalyanasundaram, J. Kiwi, M. Grätzel, *Helv. Chim. Acta* **1978**, *61*, 2720–2730.

[23] M. Landmann, E. Rauls, W. G. Schmidt, *J. Phys. Condens. Matter* **2012**, *24*, 195503.

[24] A. Fujishima, K. Honda, *Nature* **1972**, *238*, 37–38.

[25] A. L. Linsebigler, G. Lu, J. T. Yates, *Chem. Rev.* **1995**, *95*, 735–758.

[26] X. Wang, A. Kafizas, X. Li, S. J. A. Moniz, P. J. T. Reardon, J. Tang, I. P. Parkin, J. R. Durrant, *J. Phys. Chem. C* **2015**, *119*, 10439–10447.

[27] Y. Kakuma, A. Y. Nosaka, Y. Nosaka, *Phys. Chem. Chem. Phys.* **2015**, *17*, 18691–18698.

[28] B. Banerjee, V. Amoli, A. Maurya, A. K. Sinha, A. Bhaumik, *Nanoscale* **2015**, *7*, 10504–10512.

[29] V. Amoli, S. Bhat, A. Maurya, B. Banerjee, A. Bhaumik, A. K. Sinha, *ACS Appl. Mater. Interfaces* **2015**, *7*, 26022–26035.

[30] T. Kawai, T. Sakata, *J. Chem. Soc., Chem. Commun.* **1980**, 694–695.

[31] J. Wu, S. Lu, D. Ge, L. Zhang, W. Chen, H. Gu, *RSC Adv.* **2016**, *6*, 67502–67508.

[32] Q. Fan, S. He, L. Hao, X. Liu, Y. Zhu, S. Xu, F. Zhang, *Sci. Rep.* **2017**, *7*, 42172–42186.

[33] L. Guo, Z. Yang, K. Marcus, Z. Li, B. Luo, L. Zhou, X. Wang, Y. Du, Y. Yang, *Energy Environ. Sci.* **2018**, *11*, 106–114.

[34] W. Ho, J. C. Yu, J. Lin, J. Yu, P. Li, *Langmuir* **2004**, *20*, 5865–5869.

[35] B. Mahler, V. Hoepfner, K. Liao, G. A. Ozin, *J. Am. Chem. Soc.* **2014**, *136*, 14121–14127.

[36] F. Xu, L. Zhang, B. Cheng, J. Yu, *ACS Sustainable Chem. Eng.* **2018**, *6*, 12291–12298.

[37] X. Zhang, Y. Chen, Y. Xiao, W. Zhou, G. Tian, H. Fu, *Nanoscale* **2018**, *10*, 4041–4050.

[38] L. Zhang, B. Tian, F. Chen, J. Zhang, *Int. J. Hydrogen Energy* **2012**, *37*, 17060–17067.

[39] Y. Im, S. Kang, K. M. Kim, T. Ju, G. B. Han, N.-K. Park, T. J. Lee, M. Kang, *Int. J. Photoenergy* **2013**, *2013*, 1–10.

[40] S. Yu, J. Liu, Y. Zhou, R. D. Webster, X. Yan, *ACS Sustain. Chem. Eng.* **2016**, *5*, 1347–1357.

[41] M. Chandra, K. Bhunia, D. Pradhan, *Inorg. Chem.* **2018**, *57*, 4524–4533.

[42] F. Chen, W. Luo, Y. Mo, H. Yu, B. Cheng, *Appl. Surf. Sci.* **2018**, *430*, 448–456.

[43] Z. Yu, J. Meng, J. Xiao, Y. Li, Y. Li, *Int. J. Hydrogen Energy* **2014**, *39*, 15387–15393.

[44] T. Oda, M. Shirai, N. Suzuki, K. Motizuki, *J. Phys. : Condens. Matter,* **1995**, *7*, 4433–4446.

[45] R. A. D. Pattrick, V. S. Coker, C. I. Pearce, N. D. Telling, G. van der Laan, *Can. Mineral.* **2008**, *46*, 1317–1322.

[46] K. Miyatani, T. Tanaka, S. Sakita, M. Ishikawa, N. Shirakawa, *Jpn. J. Appl. Phys.* **1993**, *32*, 448–450.

[47] Y. Furukawa, S. Wada, K. Miyatani, T. Tanaka, M. Fukugauchi, M. Ishikawa, *Phys. Rev. B* **1995**, *51*, 6159–6162.

[48] S. Wada, H. Sugita, K. Miyatani, T. Tanaka, T. Nishikawa, *J. Phys. Condens. Matter* **2002**, *14*, 219–230.

[49] H. Sugita, S. Wada, K. Miyatani, T. Tanaka, M. Ishikawa, *Phys. B* **2000**, *284–288*, 473–474.

[50] A. N. Buckley, W. M. Skinner, S. L. Harmer, A. Pring, L.-J. Fan, *Geochim. Cosmochim. Acta* **2009**, *73*, 4452–4467.

[51] M. Chauhan, K. Soni, P. E. Karthik, K. P. Reddy, C. S. Gopinath, S. Deka, *J. Mater. Chem. A* **2019**, *7*, 6985–6994.

[52] S. Hariganesh, S. Vadivel, D. Maruthamani, M. Kumaravel, A. Habibi-Yangjeh, *J. Inorg. Organomet. Polym.* **2018**, *28*, 1276–1285.

[53] Y. Chen, X. Ji, V. Sethumathavan, B. Paul, *Materials* **2018**, 11:2303.

[54] Y. Lang, L. Pan, C. Chen, Y. Wang, *J. Electron. Mater.* **2019**, *48*, 4179–4187.

[55] M. Chauhan, K. P. Reddy, C. S. Gopinath, S. Deka, *ACS Catal.* **2017**, *7*, 5871–5879.

[56] Y. Ge, J. Wu, X. Xu, M. Ye, J. Shen, *Int. J. Hydrogen Energy* **2016**, *41*, 19847–19854.

[57] A. M. Wiltrout, C. G. Read, E. M. Spencer, R. E. Schaak, *Inorg. Chem.* **2016**, *55*, 221–226.

[58] B. Ohtani, O. O. Prieto-Mahaney, D. Li, R. Abe, *J. Photoch. Photobio. A* **2010**, *216*, 179–182.

[59] D. M. Tobaldi, R. C. Pullar, M. P. Seabra, J. A. Labrincha, *Mater. Lett.* **2014**, *122*, 345–347.

[60] J. Yu, H. Yu, B. Cheng, M. Zhou, X. Zhao, *J. Mol. Catal. A* **2006**, *253*, 112–118.

[61] M. Horn, C. F. Schwerdtfeger, E. P. Meagher, *Z. Kristallogr.* **1972**, *136*, 273–281.

[62] S. C. Abrahams, J. L. Bernstein, *J. Chem. Phys.* **1971**, *55*, 3206–3211.

[63] D. P. Williamson, N. W. Grimes, *J. Phys. D* **1974**, *7*, 1–6.

[64] G. Kortüm, W. Braun, G. Herzog, *Angew. Chem. Int. Ed. Engl.* **1963**, *2*, 333–341; *Angew. Chem.* **1963**, *75*, 653.

[65] P. A. Lee, G. Said, R. Davis, T. H. Lim, *Solid State Commun.* **1969**, *7*, 2719–2729.

[66] M. Thommes, K. Kaneko, A. V. Neimark, J. P. Olivier, F. Rodriguez-Reinoso, J. Rouquerol, K. S. W. Sing, *Pure Appl. Chem.* **2015**, *87*, 160–178.

[67] S. Brunaer, P. H. Emmett, E. Teller, S. Brunauer, P. H. Emmett, E. Teller, *J. Am. Chem. Soc.* **1938**, *60*, 309–319.

[68] A. L. Luna, D. Dragoe, K. Wang, P. Beaunier, E. Kowalska, B. Ohtani, D. Bahena Uribe, M. A. Valenzuela, H. Remita, C. Colbeau-Justin, *J. Phys. Chem. C* **2017**, *121*, 14302–14311.

[69] K. C. Christoforidis, P. Fornasiero, *ChemCatChem* **2017**, *9*, 1523–1544.

[70] Z. Bian, T. Tachikawa, P. Zhang, M. Fujitsuka, T. Majima, *J. Am. Chem. Soc.* **2014**, *136*, 458–465.

[71] J. S. DuChene, B. C. Sweeny, A. C. Johnston-Peck, D. Su, E. A. Stach, W. D. Wei, *Angew. Chem. Int. Ed.* **2014**, *53*, 7887–7891; *Angew. Chem.* **2014**, *126*, 8021.

[72] A. Furube, S. Hashimoto, *NPG Asia Mater.* **2017**, *9*, e454–e454.

[73] R. Katoh, A. Furube, T. Yoshihara, K. Hara, G. Fujihashi, S. Takano, S. Murata, H. Arakawa, M. Tachiya, *J. Phys. Chem. B* **2004**, *108*, 4818–4822.

[74] V. Kumaravel, M. Imam, A. Badreldin, R. Chava, J. Do, M. Kang, A. Abdel-Wahab, *Catalysts* **2019**, *9*, 276.

[75] N. Serpone, *J. Photochem. Photobiol. A* **1997**, *104*, 1–12.

[76] N. Serpone, A. Salinaro, *Pure Appl. Chem.* **1999**, *71*, 303–320.

[77] H. Kisch, D. Bahnemann, *J. Phys. Chem. Lett.* **2015**, *6*, 1907–1910.

[78] M. J. Muñoz-Batista, A. Kubacka, A. B. Hungría, M. Fernández-García, *J. Catal.* **2015**, *330*, 154–166.

[79] M. Qureshi, K. Takanabe, *Chem. Mater.* **2016**, *29*, 158–167.

[80] X. Zhang, M. Yang, J. Zhao, L. Guo, *Int. J. Hydrogen Energy* **2013**, *38*, 15985–15991.

[81] Z. Jin, X. Zhang, G. Lu, S. Li, *J. Mol. Catal. A* **2006**, *259*, 275–280.

[82] W. Zhen, W. Jiao, Y. Wu, H. Jing, G. Lu, *Catal. Sci. Technol.* **2017**, *7*, 5028–5037.

[83] K. Dai, X. Zhang, K. Fan, P. Zeng, T. Peng, *J. Nanomater.* **2014**, *2014*, 694073.

EurJIC
European Journal of Inorganic Chemistry

Full Paper
doi.org/10.1002/ejic.202000555

Chemistry Europe
European Chemical
Societies Publishing

[84] M. Wang, S. Shen, L. Li, Z. Tang, J. Yang, *J. Mater. Sci.* **2017**, *52*, 5155–5164.

[85] P. Ganesan, A. Sivanantham, S. Shanmugam, *ACS Appl. Mater. Interfaces* **2017**, *9*, 12416–12426.

[86] Y. Liu, H. Yu, X. Quan, S. Chen, H. Zhao, Y. Zhang, *Sci. Rep.* **2014**, *4*, 6843.

[87] L. Forro, O. Chauvet, D. Emin, L. Zuppiroli, H. Berger, F. Lévy, *J. Appl. Phys.* **1994**, *75*, 633–635.

[88] D. Mardare, G. I. Rusu, *J. Non-Cryst. Solids* **2010**, *356*, 1395–1399.

[89] I. Oja, A. Mere, M. Krunks, R. Nisumaa, C.-H. Solterbeck, M. Es-Souni, *Thin Solid Films* **2006**, *515*, 674–677.

[90] F. Yakuphanoglu, *Solid State Sci.* **2012**, *14*, 673–676.

[91] R. Amade, P. Heitjans, S. Indris, M. Finger, A. Haeger, D. Hesse, *Phys. Chem. Chem. Phys.* **2006**, *8*, 777–782.

[92] S. Indris, R. Amade, P. Heitjans, M. Finger, A. Haeger, D. Hesse, W. Grünert, A. Börger, K. D. Becker, *J. Phys. Chem. B* **2005**, *109*, 23274–23278.

[93] T. Giannakopoulou, I. Papailias, N. Todorova, N. Boukos, Y. Liu, J. Yu, C. Trapalis, *Chem. Eng. J.* **2017**, *310*, 571–580.

[94] M. S. Lee, I. C. Cheon, Y. I. Kim, *Bull. Korean Chem. Soc.* **2003**, *24*, 1155–1162.

[95] M. R. Simond, K. Ballerat-Busserolles, Y. Coulier, L. Rodier, J.-Y. Coxam, *J. Solution Chem.* **2012**, *41*, 130–142.

[96] B. W. Mountain, T. M. Seward, *Geochim. Cosmochim. Acta* **1999**, *63*, 11–29.

[97] S. B. Romberger, H. L. Barnes, *Econ. Geol.* **1970**, *65*, 901–919.

[98] D. Shea, G. R. Helz, *Geochim. Cosmochim. Acta* **1988**, *52*, 1815–1825.

[99] D. Shea, G. R. Helz, *Geochim. Cosmochim. Acta* **1989**, *53*, 229–236.

[100] J. Xing, J. F. Chen, Y. H. Li, W. T. Yuan, Y. Zhou, L. R. Zheng, H. F. Wang, P. Hu, Y. Wang, H. J. Zhao, Y. Wang, H. G. Yang, *Chemistry* **2014**, *20*, 2138–2144.

[101] L. Wang, X. Duan, G. Wang, C. Liu, S. Luo, S. Zhang, Y. Zeng, Y. Xu, Y. Liu, X. Duan, *Appl. Catal. B* **2016**, *186*, 88–96.

[102] Q. Liu, X. Li, Q. He, A. Khalil, D. Liu, T. Xiang, X. Wu, L. Song, *Small* **2015**, *11*, 5556–5564.

[103] C. Liu, L. Wang, Y. Tang, S. Luo, Y. Liu, S. Zhang, Y. Zeng, Y. Xu, *Appl. Catal. B* **2015**, *164*, 1–9.

[104] C. Yang, J. Qin, Z. Xue, M. Ma, X. Zhang, R. Liu, *Nano Energy* **2017**, *41*, 1–9.

[105] InfoMine Inc., *Palladium price*, http://www.infomine.com/investment/metal-prices/palladium/5-year/, Accessed on **2018**/10/09.

[106] InfoMine Inc., *Cobalt price*, http://www.infomine.com/investment/metal-prices/cobalt/5-year/, Accessed on **2018**/10/09.

[107] Q. Wang, G. Yun, Y. Bai, N. An, Y. Chen, R. Wang, Z. Lei, W. Shangguan, *Int. J. Hydrogen Energy* **2014**, *39*, 13421–13428.

[108] Alan Coelho, *Topas Academic v6*, Coelho Software, **2016**.

[109] *jEdit*, http://www.jedit.org/index.php?page=features, Accessed on **2018**/11/21.

[110] D. R. G. Mitchell, *Microsc. Res. Tech.* **2008**, *71*, 588–593.

[111] P. A. Stadelmann, *Ultramicroscopy* **1987**, *21*, 131–145.

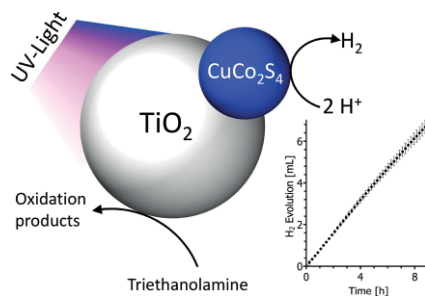[112] H. J. Kuhn, S. E. Braslavsky, R. Schmidt, *Pure Appl. Chem.* **2004**, *76*, 2105–2146.

Photocatalysis

*M. Poschmann, H. Groß, R. Amin,
C. Fritsch, T. Dankwort, H. Radinger,
S. Indris, L. Kienle, W. Bensch* 1–12*

CuCo$_2$S$_4$ Deposited on TiO$_2$: Controlling the pH Value Boosts Photocatalytic Hydrogen Evolution

Nanosized metallic CuCo$_2$S$_4$ deposited on TiO$_2$ shows high photocatalytic hydrogen evolution using triethanolamine as sacrificial agent. Controlling the pH value boosts the photocatalytically produced amount of hydrogen. An enormous long-term stability of the composite is obtained at neutral pH value.

doi.org/10.1002/ejic.202000555